SUPPORTING INFORMATION

Multimodal theranostic nanoformulations permit magnetic resonance bioimaging of antiretroviral drug particle tissue-cell biodistribution

Bhavesh D. Kevadiya[1], Christopher Woldstad[2], Brendan M. Ottemann[1], Prasanta Dash[1], Balasrinivasa R. Sajja[2], Benjamin Lamberty[1], Brenda Morsey[1], Ted Kocher[1], Rinku Dutta[1], Aditya N. Bade[1], Yutong Liu[2], Shannon E. Callen[1], Howard S. Fox[1], Siddappa N. Byrareddy[1], JoEllyn M. McMillan[1], Tatiana K. Bronich[3], Benson J. Edagwa[1], Michael D. Boska[2] and Howard E. Gendelman[1,*]

[1]*Department of Pharmacology and Experimental Neuroscience, University of Nebraska Medical Center, Omaha, NE, USA*
[2]*Department of Radiology, University of Nebraska Medical Center, Omaha, NE, USA*
[3]*Department of Pharmaceutical Sciences, University of Nebraska Medical Center, Omaha, NE, USA*

[*]Corresponding authors: Howard E. Gendelman, M.D., Department of Pharmacology and Experimental Neuroscience, University of Nebraska Medical Center, Omaha, NE 68198;
Phone 402 559 8920; FAX: 402 559 3744; Email: hegendel@unmc.edu

Method

Cell fixation and block preparation method for electron microscopy

MDM (1.5 x 10^6 cells/mL) were incubated for 8 h with EuCF-DTG and FA-EuCF-DTG nanoparticles (5 µg/mL). For TEM, MDM were fixed in a solution of 2% glutaraldehyde and 2% paraformaldehyde in 0.1 M Sorenson's phosphate buffer (pH 6.2) for 24 h at 4°C. Samples were washed three times with PBS. During processing samples were post-fixed in a 1% aqueous solution of osmium tetroxide for 30 minutes. Subsequently, samples were dehydrated in a graded ethanol and propylene oxide used as a transition solvent between the ethanol and araldite resin. Samples were allowed to sit overnight in a 50:50 propylene oxide:resin solution until all the propylene oxide had evaporated then they were incubated in fresh resin for 2 h at room temperature before embedding. Polymerization took place at 65°C for 24 h. The staining procedure was 10 minutes in 2% (w/v) uranyl acetate, washed 3 times in distilled water, 10 minutes in Reynolds Lead Citrate, and washed 3 times in distilled water. Thin sections (100nm) made with Leica UC6 Ultracut ultramicrotome were placed on 200 mesh copper grids, and examined on the Tecnai G2 Spirit TWIN (FEI) operating at 80kV. Images were acquired digitally with an AMT imaging system.

For SEM MDM (1x10^6 cells/mL) were grown on Thermonox coverslips in 6 well plate for 8 h with EuCF-DTG nanoparticles (5 µg/mL). After EuCF-DTG nanoparticles treatment the cells were fixed with 2% glutaraldehyde and 2% paraformaldehyde in 0.1M Sorensen's phosphate buffer. Cell samples were washed 3 times 10 minutes each in buffer, post-fixed in 1% osmium tetroxide aqueous solution for 30minutes, washed 3 times 10 minutes each in buffer. Samples were then dehydrated through a graded ethanol series 50, 70, 90, 95, and 100% 3 times for 10 minutes each. Then the samples were washed 3 times in 100% hexamethyldisilazane (HMDS) for 10 minutes each. Finally samples were left in 100% HMDS overnight in a fume hood to allow for complete evaporation. Samples were mounted on SEM stubs and Sputter Coater with a layer of gold/palladium 50 nm thick. Samples were observed on a FEI Quanta 200 SEM. The particulate suspension sample a drop of which was placed on a SEM stub and allowed to air dry.

DTG quantitation and cell distribution

Drug content in cell extracts was measured using a Waters ACQUITY H-Class ultra-performance liquid chromatography (UPLC) system with Empower 3 software, Milford, MA, USA. Cell extracts were separated on a Phenomenex Kinetex 5 µm C18 columns (150 X 4.6 mm, Phenomenex Ltd., Torrance, CA, USA) using an isocratic mobile phase of 65% 50 mM KH_2PO_4, pH 3.2 / 35% acetonitrile at a flow rate of 1.0 mL/min and detection at 254 nm. Drug content was quantitated by comparison of the peak area to those of known standards (determined at 0.05–50 µg/mL).

Plasma and tissue drug, iron and cobalt animal tissue quantifications

Drug concentrations in animal plasma and tissues were determined by UPLC-tandem mass spectrometry (UPLC-MS/MS) using a Waters Acquity H-class UPLC- Xevo TQ-S micro system (Waters Corp, Milford, MA, USA). For plasma drug quantitation, 25 µL of sample was added into 1 mL acetonitrile, followed by addition of 10 µL of internal standard (IS) solution to achieve a final IS concentration of 50 ng/mL DTG-d3 (Clearsynth Canada Inc, Mississauga, ON, Canada) after reconstitution. Samples were

then vortexed and centrifuged at 17,000 g for 10 min at 4°C. Supernatants were dried using a Thermo Scientific Savant Speed Vacuum (Waltham, MA) and reconstituted in 100 µL 50% (v/v) acetonitrile in MS-grade water. Standard curves were prepared in blank rat plasma in the range of 0.2–00 ng/mL. For tissue analyses, 100 mg of tissue was homogenized in 4 volumes of 90% (v/v) acetonitrile in MS-grade water using a Qiagen Tissue Lyzer II (Valencia, CA, USA). To 100 µL of tissue homogenate 80 µL of acetonitrile, 10 µL of 50% acetonitrile (v/v) was added in MS-grade water, and 10 µL IS. Standard curve samples were prepared using equivalent tissue matrix dilutions, 80 µL of acetonitrile, 10 µL of 50% acetonitrile (v/v) in MS-grade water spiked with standard drug concentrations, and 10 µL of IS. Chromatographic separation of 10 µL of plasma or tissue samples was achieved with an ACQUITY UPLC-BEH Shield RP18 column (1.7 µm, 2.1 mm x 100 mm) using a 10-min gradient of mobile phase A (7.5 mM ammonium formate in Optima-grade water adjusted to pH 3 using formic acid) and mobile phase B (100% Optima-grade acetonitrile) at a flow rate of 0.25 mL/min. The initial mobile phase composition of 40% B was held for the first 3 min, increased to 86% B over 0.5 min further, held constant for 5 min, then reset to 40% B over 0.25 min and held constant for 1.25 min. DTG was detected at a cone voltage of 10 volts and collision energy of 25 volts. Multiple reaction monitoring (MRM) transitions used for DTG and DTG-d3 were 420.075 > 277.124 and 422.841 > 129.999 m/z, respectively. Spectra were analyzed and quantified by Mass Lynx software version 4.1. DTG quantitations were based upon drug peak area to internal standard peak area ratios. Iron and cobalt levels were quantified by inductively coupled plasma mass spectrometry (ICP-MS) on an Agilent Technologies ICP-MS 7500cs (Santa Clara, CA) and an ESI SC-4 high-throughput autosampler (Elemental Scientific Inc., Omaha, NE) [1].

Immunocytochemistry of rhesus macaque tissues

Tissues (spleen and lymph nodes) were perfused with phosphate buffer saline (PBS) followed by post-fixation with 4% paraformaldehyde (PFA) for 3 days at room temperature then processed in a automated processor in Shandon Citadel-1000 processor (Thermo scientific) for 18 h with reagents in step-wise manner containing 70, 95 and 100% flex followed by Xylene and paraffin. Finally tissues were embedded using paraffin blocks for further sectioning. Sections 5µ-thick were cut from the paraffin blocks, mounted on glass slides and labelled with combination of rabbit monoclonal antibody to CD68 (Sigma-Aldrich, St. Louis, MO, USA) for macrophages and mouse monoclonal antibodies to SIV-p27. Primary antibodies were labeled with secondary anti-mouse and anti-rabbit antibodies conjugated to the fluorescent probes Alexa Fluor® 633 and Alexa Fluor®594 and nuclei were labeled with 4′,6-diamidino-2-phenylindole (DAPI). Slides were cover slipped with ProLong Gold anti-fade reagent (Invitrogen, Carlsbad, CA), allowed to dry for 24 h at room temperature and then stored at −20 °C for future use. Images were captured at wavelengths encompassing the emission spectra of probes, with a 40X magnification objective. Images were captured using a Zeiss LSM710 confocal microscope and analyzed with Zen 2011 software (Carl Zeiss Micro imaging).

Results

Nanoparticle characterizations

FA-EuCF-DTG nanoparticles were used in rapid, real-time screening of nanoformulation tissue drug biodistribution[2, 3]. The multimodal-targeted drug delivery system contain in shell cationic lipids, PC, DSPE-PEG_{2000} and DOPE improve biocompatibility, reduce toxicity, and increase hydrophobic drug carrying capacities[4-6]. Attaching FA to the lipid

surface increase macrophage uptake and retention of nanoparticles over time [7-10]. Targeting ligand moieties affect the efficiency of theranostic probes to evaluate nanoformulated ARV biodistribution[8, 11, 12]. The lipid shell provide nanoparticle stability and size uniformity for three weeks at 4°C (Figure S1).

MRI screening of nanoparticles administered to rats

FA-EuCF-DTG nanoparticles were administered to the smaller group of rats (N=10) for investigating the effect of nanoparticle decoration on nanoparticle biodistribution (Figure S9A-C). Rats administered with FA-EuCF-DTG nanoparticles showed significantly higher concentrations of iron and cobalt within the liver and spleen compared to rats given EuCF-DTG nanoparticles (Figure S9C and S10A-C). Higher cobalt levels were seen within the liver, spleen, lymph nodes, and gastrointestinal tract indicating effects of FA targeting on nanoparticle biodistribution systematically (Figure S10B-C).

MRI screening of EuCF-DTG nanoparticles in rhesus macaques

T_2 relaxation times differences between pre- and 5 days post-injection were observed within the spleen of rats and rhesus macques models, with rhesus macaques showing spleen T_2 values of 102.9 ms in pre-images and 98.66 ms in post-images, and rats showing spleen T_2 values of 56.37 ms in pre-images and 49.10 ms in post-images (data not shown).

Cobalt and DTG concentrations in rats and rhesus macaques

Plasma cobalt concentrations of EuCF-DTG nanoparticles followed by IV injection in rats were found to be 49.10 ± 3.93 and 5.68 ± 0.7 ng/mL at days 1 and 5, respectively. EuCF-DTG nanoparticles IM injected rats showed a slower decline to 36.48 ± 9.33, 24.45 ± 8.22 and 16.03 ± 10.77 ng/mL at days 1, and 5, respectively (Figure S10D). Although, DTG plasma concentrations in IV injected rats were 3147.8 ± 64, 913.0 ± 41, 39.0 ± 31 and 1.6 ± 0.7 ng/mL at days 1, 2, 5 and 10, respectively. IM injected rats showed a slower decline to 3863 ± 29, 1288 ± 33, 474 ± 80 and 14.6 ± 2 ng/mL at days 1, 2, 5 and 10, respectively (Figure S10E). Concentrations of DTG within post-mortem liver and spleen tissues after administration of FA-EuCF-DTG were 17.5 ng/g in liver and 28.0 ng/g after IV administration and 12.0 ng/g in liver and 17.5 ng/g after IM administration in spleen (data not shown). While concentrations of DTG within the plasma of rhesus macaques showed a gradual decrease over time, with plasma DTG levels of 49.9 and 31.1 ng/mL at days 3 and 7 (Figure S14E). Concentrations of DTG within the tissues of rhesus macaques were 40.5, 27.0, 8.0, 8.0 and 1.5 ng/g in liver, kidney, spleen, lymph node and lung, respectively (Figure S14F). Cobalt levels in the tissues of rhesus macaques following same pattern as DTG concentrations in tissues (Figure S14G-H).

Nanoparticle toxicological evaluations in rats

To determine whether the EuCF-DTG nanoparticles induced any systemic toxicity, blood and tissues samples were collected and analyzed for serum metabolites and histology. No significant differences were observed for metabolic parameters (Figure S13A). Histological examination of rat liver, spleen, kidney and brain at 0, 2, 5, and 10 days showed no pathological abnormalities following EuCF-DTG nanoparticle administration (Figure S13B).

Immunocytochemistry of rhesus macaque's tissues

To define a potential macrophage localization of the EuCF-DTG nanoparticles in tissue CD68 immunostaining was performed by confocal microscopic evaluations. All images were captured with a LSM710 confocal microscope (40x objective) and Co-localization of nanoparticles with macrophages is shown in Figure S15. Histological analysis of

tissues and metabolic panels from three rhesus macaques (Figure S16 and Table S2) revealed no pathological changes in liver, spleen, lung, kidney, brain, lymph nodes and gut.

Supporting References

1. Malinouski M, Hasan NM, Zhang Y, Seravalli J, Lin J, Avanesov A, et al. Genome-wide RNAi ionomics screen reveals new genes and regulation of human trace element metabolism. 2014; 5: 3301.
2. Woods A, Patel A, Spina D, Riffo-Vasquez Y, Babin-Morgan A, de Rosales RTM, et al. In vivo biocompatibility, clearance, and biodistribution of albumin vehicles for pulmonary drug delivery. Journal of Controlled Release. 2015; 210: 1-9.
3. Ding H, Wu F. Image Guided Biodistribution and Pharmacokinetic Studies of Theranostics. Theranostics. 2012; 2: 1040-53.
4. Erten A, Wrasidlo W, Scadeng M, Esener S, Hoffman RM, Bouvet M, et al. Magnetic resonance and fluorescence imaging of doxorubicin-loaded nanoparticles using a novel in vivo model. Nanomedicine: Nanotechnology, Biology and Medicine. 2010; 6: 797-807.
5. Huang H-C, Chang P-Y, Chang K, Chen C-Y, Lin C-W, Chen J-H, et al. Formulation of novel lipid-coated magnetic nanoparticles as the probe for in vivo imaging. Journal of Biomedical Science. 2009; 16: 86.
6. Linemann T, Thomsen LB, Du Jardin KG, Laursen JC, Jensen JB, Lichota J, et al. Development of a Novel Lipophilic, Magnetic Nanoparticle for in Vivo Drug Delivery. Pharmaceutics. 2013; 5: 246-60.
7. Puligujja P, Balkundi SS, Kendrick LM, Baldridge HM, Hilaire JR, Bade AN, et al. Pharmacodynamics of long-acting folic acid-receptor targeted ritonavir-boosted atazanavir nanoformulations. Biomaterials. 2015; 41: 141-50.
8. Li T, Gendelman HE, Zhang G, Puligujja P, McMillan JM, Bronich TK, et al. Magnetic resonance imaging of folic acid-coated magnetite nanoparticles reflects tissue biodistribution of long-acting antiretroviral therapy. International Journal of Nanomedicine. 2015; 10: 3779-90.
9. Gautam N, Puligujja P, Balkundi S, Thakare R, Liu XM, Fox HS, et al. Pharmacokinetics, biodistribution, and toxicity of folic acid-coated antiretroviral nanoformulations. Antimicrob Agents Chemother. 2014; 58: 7510-9.
10. Puligujja P, McMillan J, Kendrick L, Li T, Balkundi S, Smith N, et al. Macrophage folate receptor-targeted antiretroviral therapy facilitates drug entry, retention, antiretroviral activities and biodistribution for reduction of human immunodeficiency virus infections. Nanomedicine. 2013; 9: 1263-73.
11. Kevadiya BD, Bade AN, Woldstad C, Edagwa BJ, McMillan JM, Sajja BR, et al. Development of europium doped core-shell silica cobalt ferrite functionalized nanoparticles for magnetic resonance imaging. Acta Biomaterialia. 2017; 49: 507-20.
12. Guo D, Li T, McMillan J, Sajja BR, Puligujja P, Boska MD, et al. Small magnetite antiretroviral therapeutic nanoparticle probes for MRI of drug biodistribution. Nanomedicine (Lond). 2014; 9: 1341-52.

SUPPORTING FIGURES

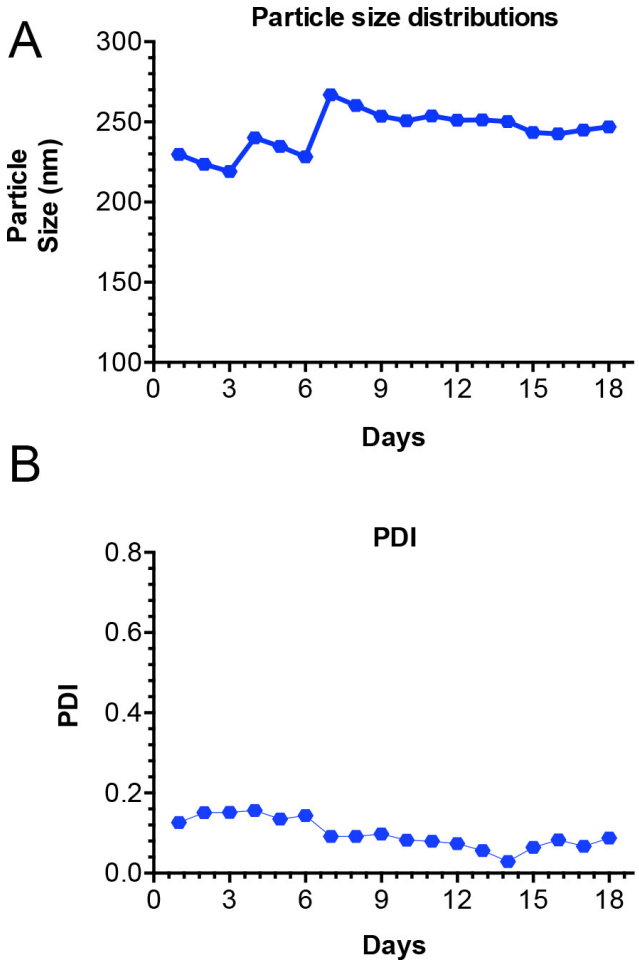

Figure S1:Nanoparticle stability measurements. (A) Average hydrodynamic size distributions of EuCF-DTG nanoparticles and (B) PDI of nanoparticles by DLS at 4°C in PBS.

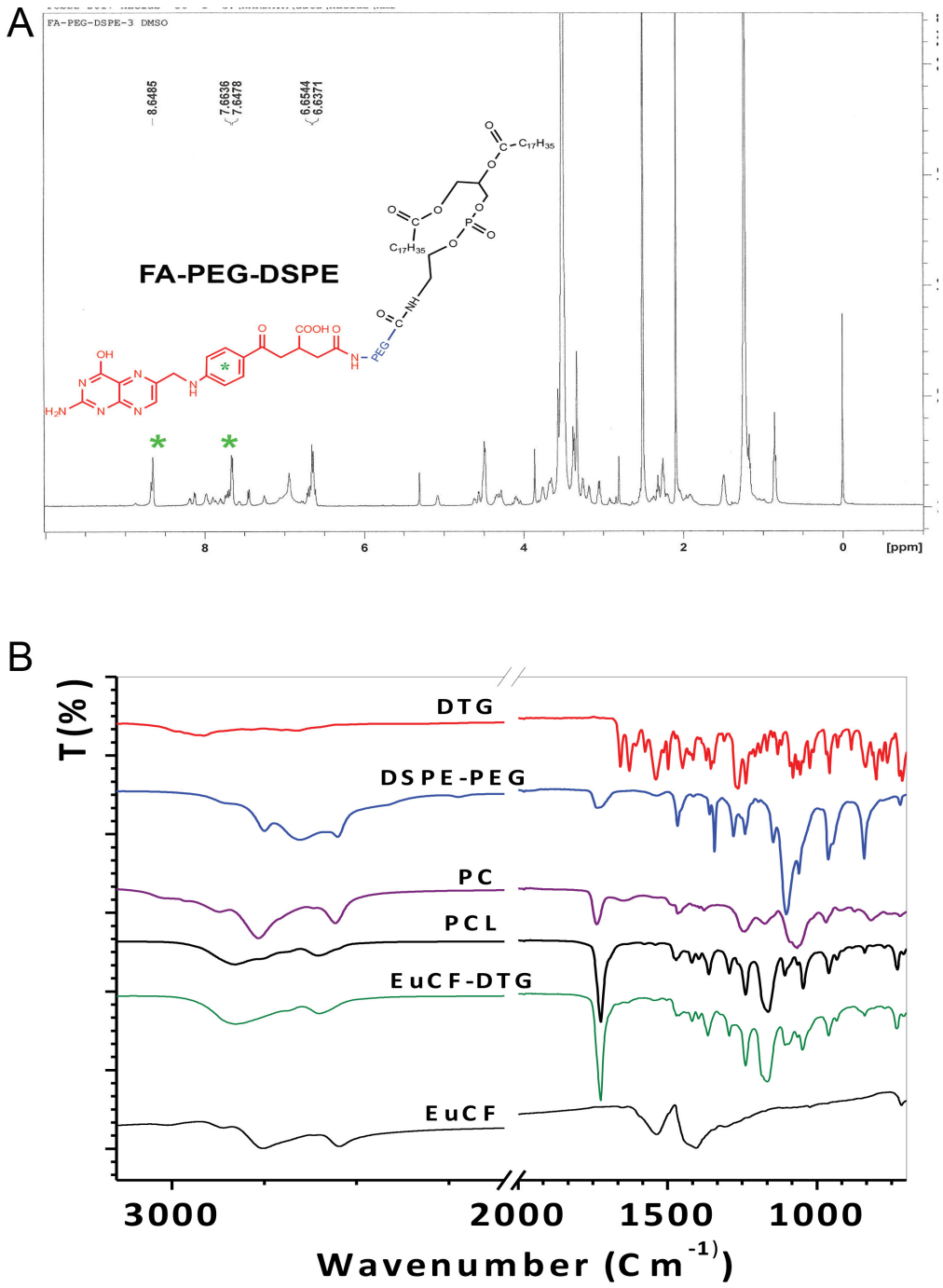

Figure S2: Characterizations of the EuCF-DTG nanoparticles by spectroscopy. (A) ^{1}H-NMR spectrum of folic acid (FA)-PEG-DSPE conjugate. Green stars indicate aromatic ring of folic acid structure and (B) Analysis of nanoparticle surface integrity by FTIR spectroscopy.

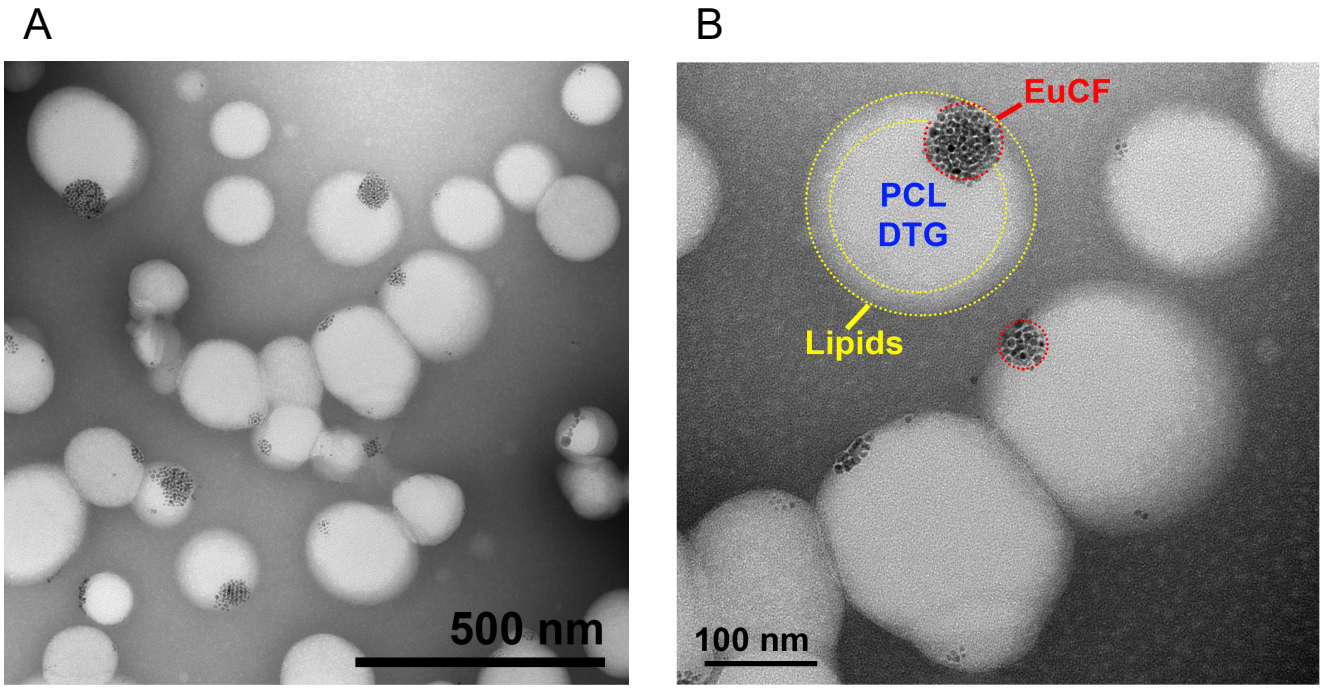

Figure S3: (A) Low-power and (B) high-power TEM of EuCFG-DTG nanoparticles.

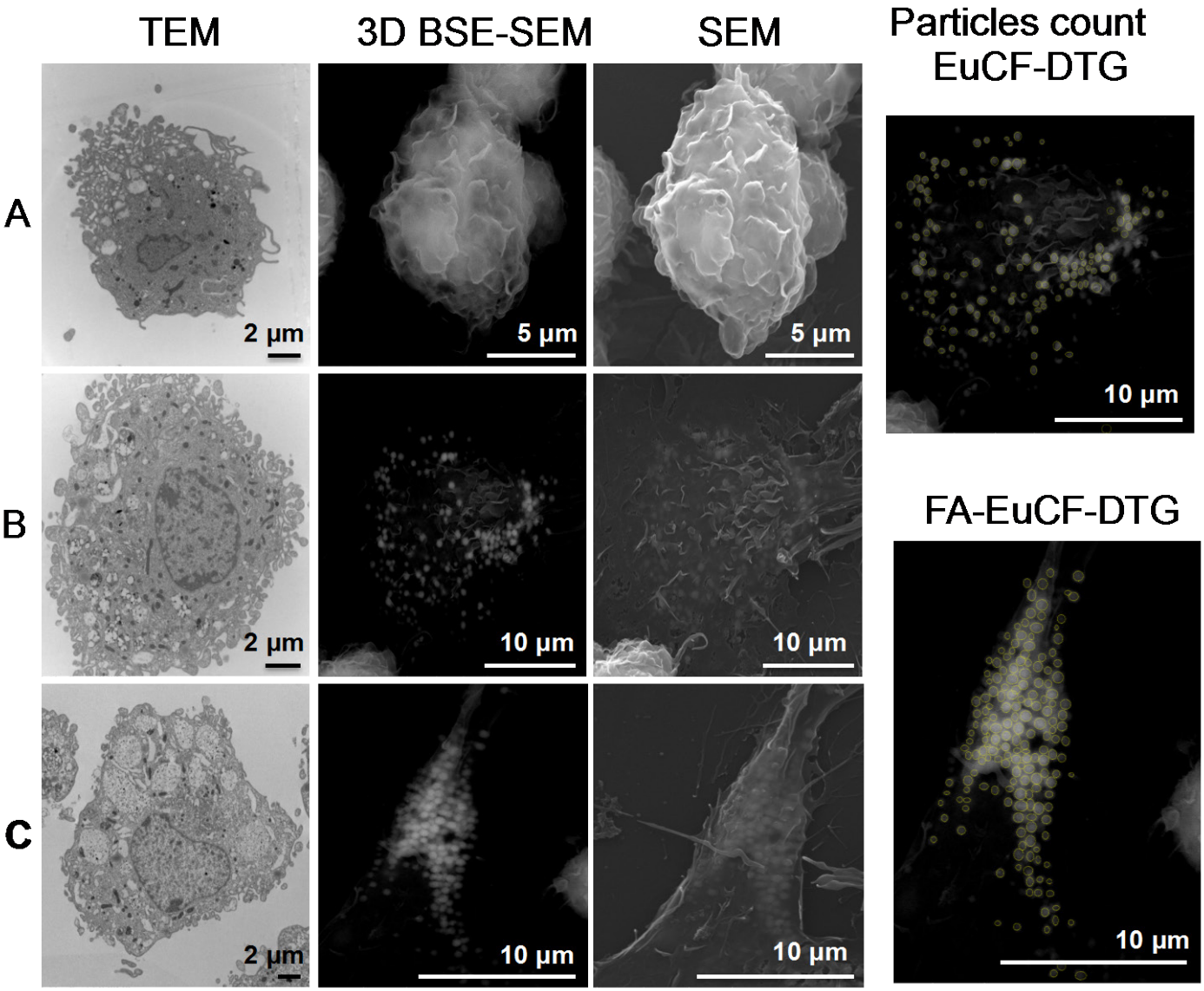

Figure S4: TEM with SEM and 3D back-scattered electron detector (BSE) images: Internal and surface morphologies of nanoparticles administered to macrophages. The TEM with SEM and 3D BSE detector images were generated with higher number of nanoparticles provides a brighter BSE intensity spot based on the electron density phases. (A) Typical morphology of a control MDM after treament with (B) EuCF-DTG and (C) FA-EuCF-DTG nanoparticles.

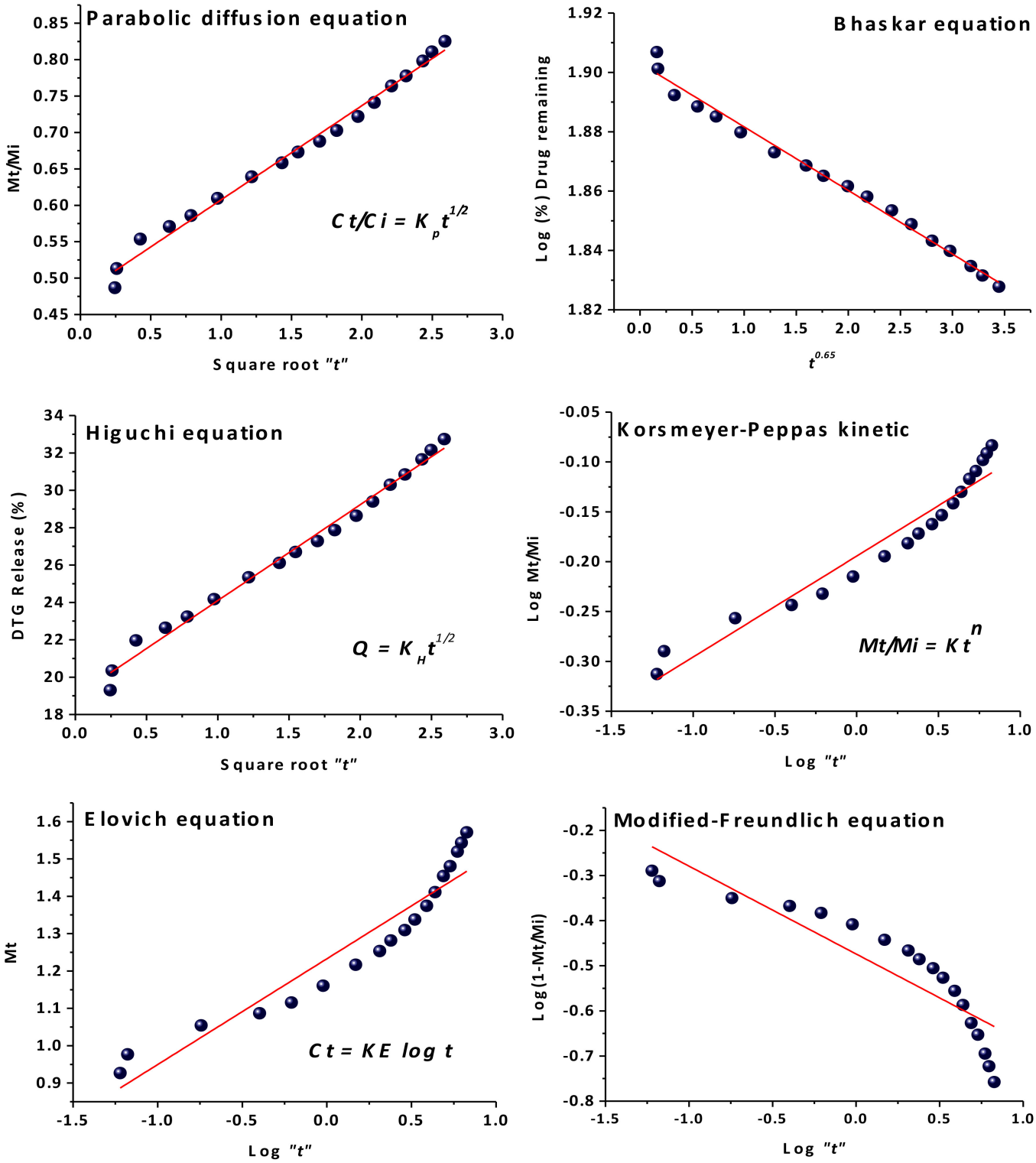

Figure S5: **Drug Release kinetic models:** Fitting the DTG release data (Figure 1F) to parabolic diffusion, Bhaskar-Equation, Higuchi, Korsmeyer–Peppas, Elovich equation and Modified-Freundlich models.

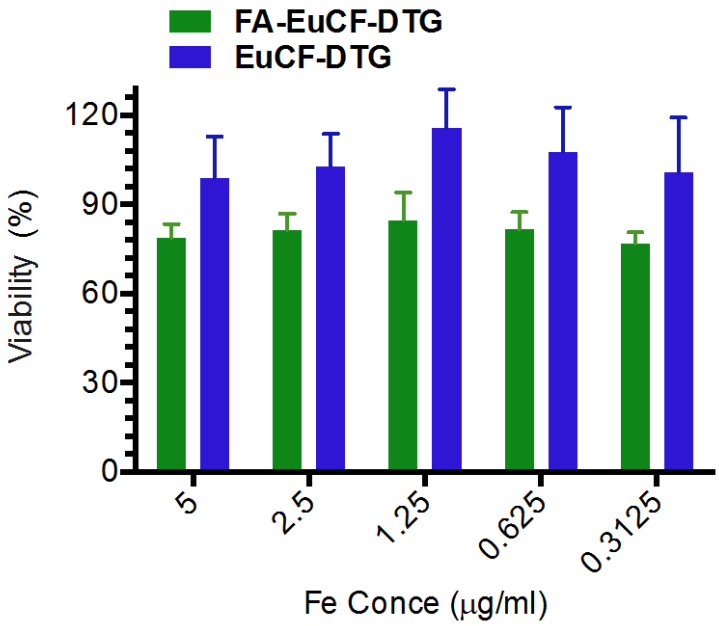

Figure S6: Cytotoxicity tests. MDM were plated in 96-well plates (80 X 10^5 cells/well) and treated with nanoparticles at increasing concentrations for 12 h. After treatment, media was removed and 100 µL of MTT solution (5 mg/mL) was added to each well. Plates were incubated at 37°C for 45 minutes. The MTT solution was removed after incubation and 200 µL of sterile DMSO was added into each well. Absorbance was measured at 490 nm.

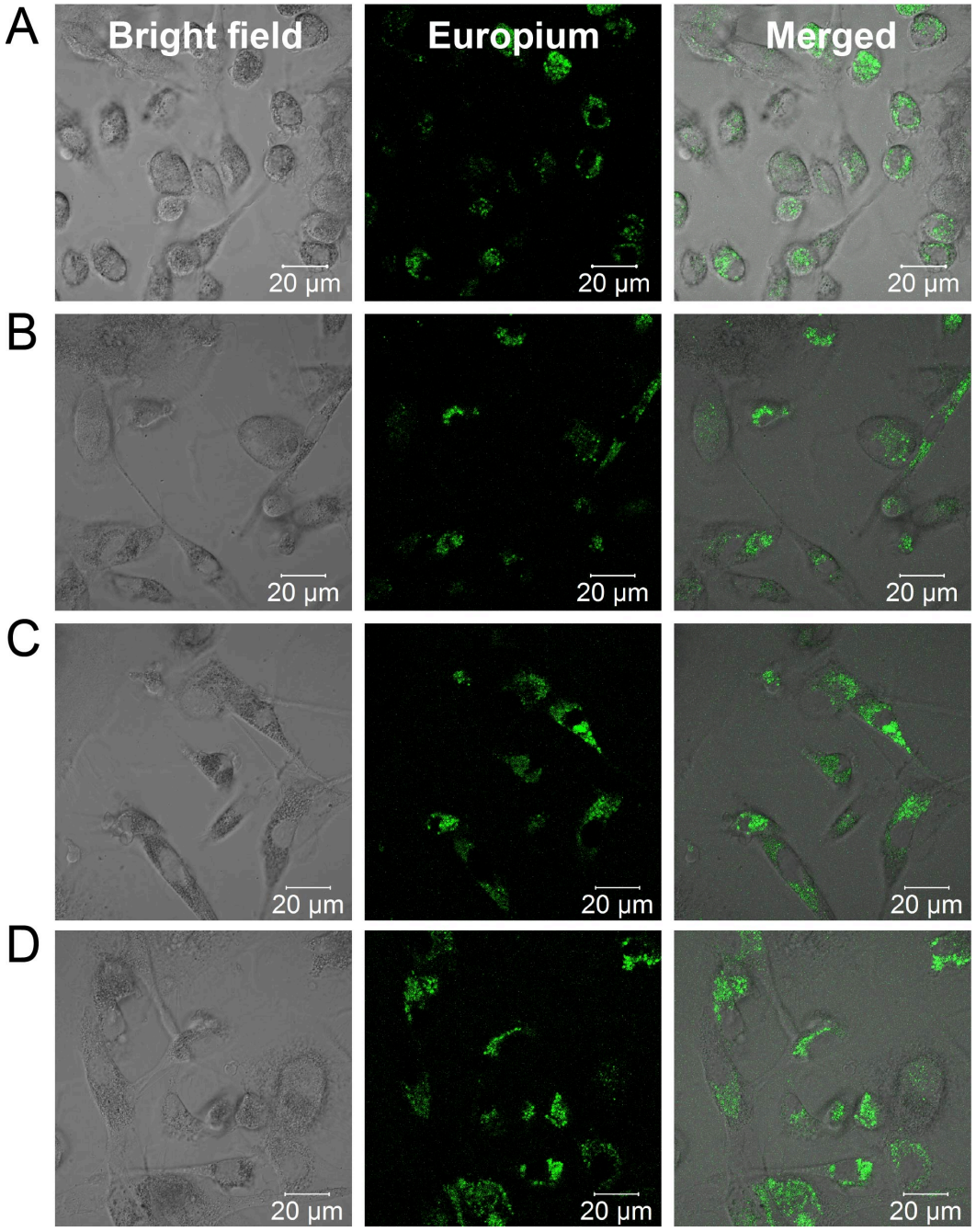

Figure S7: Time dependent uptake of nanoparticles by live cell confocal imaging. EuCF-DTG and FA-EuCF-DTG nanoparticles were added to human MDM at 5 µg/mL based on iron concentration. Concentration dependent MDM uptake of nanoparticles (A) EuCF-DTG, (B) FA-EuCF-DTG at 3 h, (C) EuCF-DTG and (D) FA-EuCF-DTG at 6 h time points are illustrated.

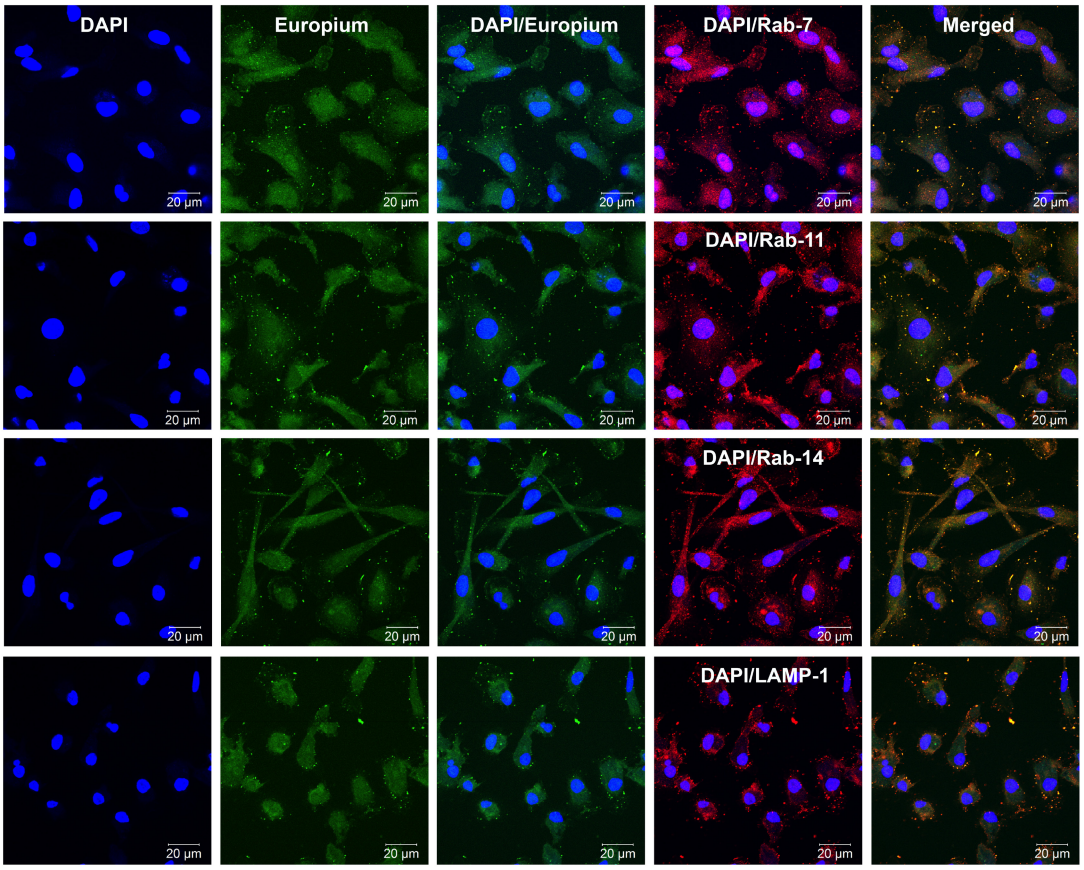

Figure S8: Subcellular distribution of EuCF-DTG nanoparticles. MDM were treated with EuCF-DTG (5 µg/mL based on iron concentrations) for 8 h and then immunostained with Rab7, -11, -14, LAMP-1 antibodies and Alexa Fluor 594-labeled secondary antibodies (red) to visualize nanoparticle and organelle co-registration. The yellow overlap (merged) shows nanoparticles (green, EuCF) and Rab compartments. DAPI (blue) stain indicates cell nuclei.

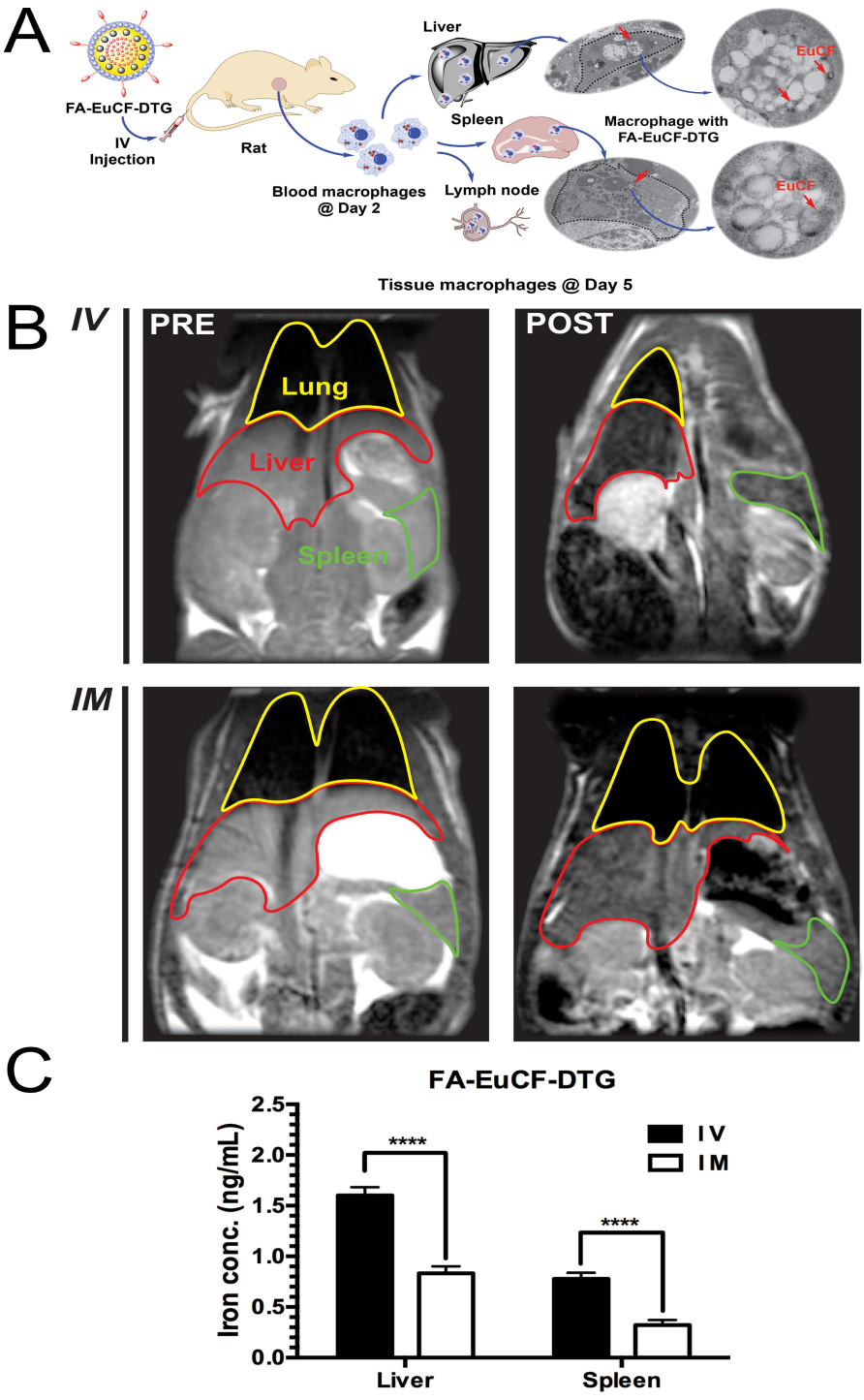

Figure S9: **FA-EuCF-DTG nanoparticle biodistribution**: (A) Schematic diagram of macrophage-based biodistribution of particles in rats reticuloendothelial system (IV: intra intravenous). Nanoparticles were administrated in Male Sprague Dawley rats followed by IV or IM injection and underwent MRI scanning immediately before injection as well as 2 and 5 days post-injection. (B) MR images of rats at day 5 after IM/IV administration of 2 mg iron/kg FA-EuCF-DTG particles (yellow: lung; red: liver; green: spleen). (C) MRI T_2 mapping again quantified the iron concentrations in the liver and spleen. Statistical differences were determined using one-way ANOVA among groups; followed by Student's t-test. (****$p < 0.0001$).

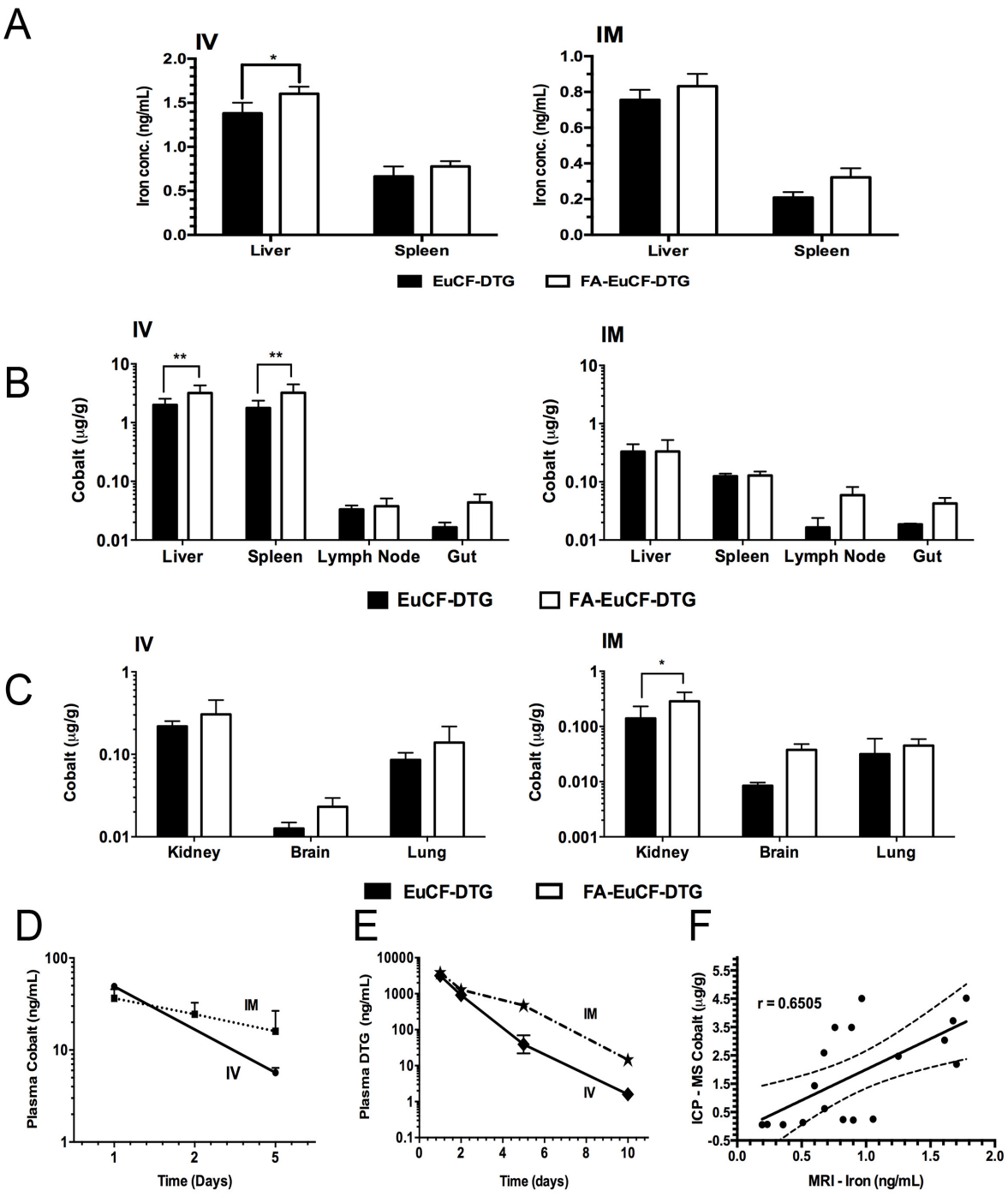

Figure S10: Biodistribution of FA-EuCF-DTG nanoparticles in rats. (A) Iron level comparisons for EuCF-DTG and FA-EuCF-DTG nanoparticle in liver and spleen measured by MRI. (B) Cobalt concentrations within lymphoid tissues and (C) brain, kidney and lung cobalt levels measured by ICPMS. (D) Plasma cobalt and (E) DTG concentrations were measured after IV or IM administration for EuCF-DTG nanoparticles. (F) Pearson's correlation in liver and spleen tissues of cobalt levels (determined by ICPMS) in tissues as compared to iron levels determined by MRI five days after injection of EuCF-DTG nanoparticles (2 mg iron/kg). Statistical differences were determined using two-way ANOVA among groups. (*$p < 0.01$; **$p < 0.001$).

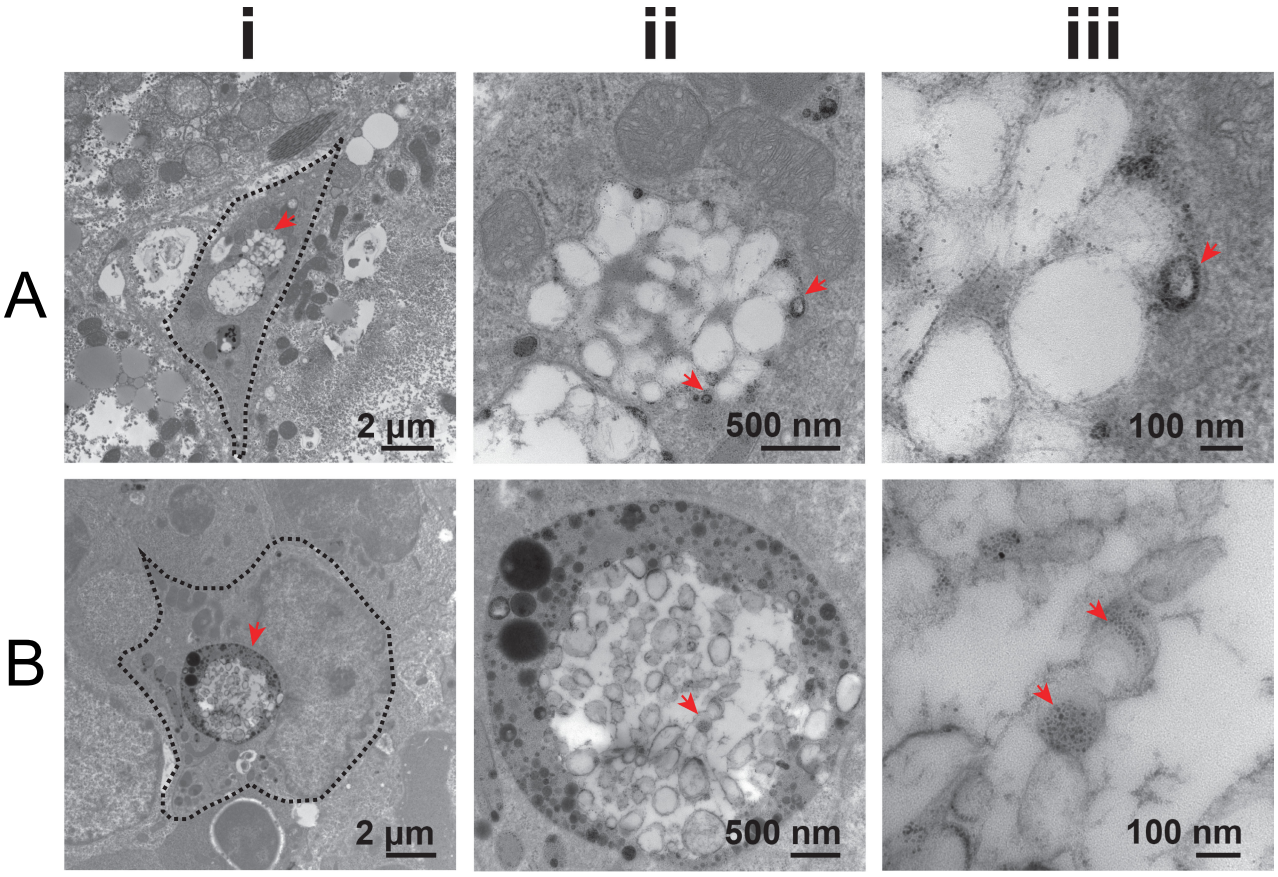

Figure S11: Morphological localization of FA-EuCF-DTG nanoparticles in rat reticuloendothelial tissues by TEM. TEM images of tissue sections of (A) liver and (B) spleen of rats after day 5 IV injection of FA-EuCF-DTG nanoparticles at 2 mg/kg of iron in rats. Panels (ii) and (iii) are higher powered images from regions indicated by red arrowheads in panel (i). Presence of nanoparticles (black dots) is clearly seen as uptakes by activated macrophages in both liver and spleen (panels ii and iii).

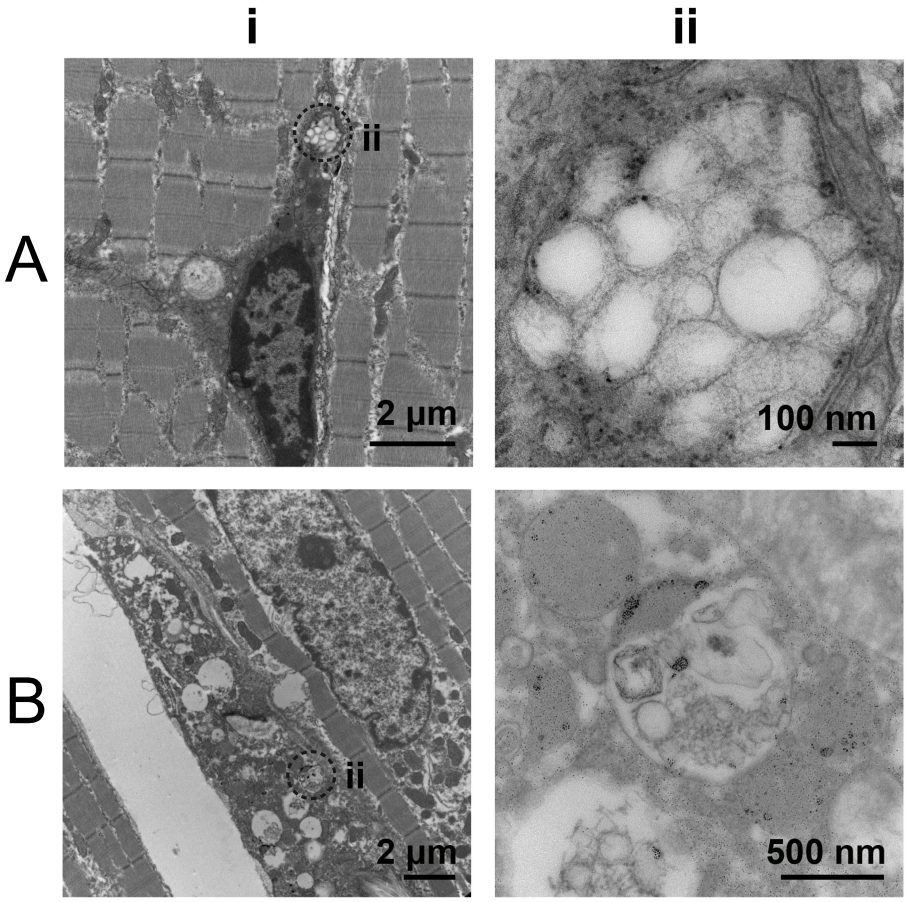

Figure S12: EuCF-DTG nanoparticles observed at the muscle injection sites. TEM images of muscle tissue of (A) non-injection site and (B) site of injection at 10-days post IM injection of 2 mg/kg based on iron content of EuCF-DTG nanoparticles, where in; (i) = low-power and (ii) = high-power images.

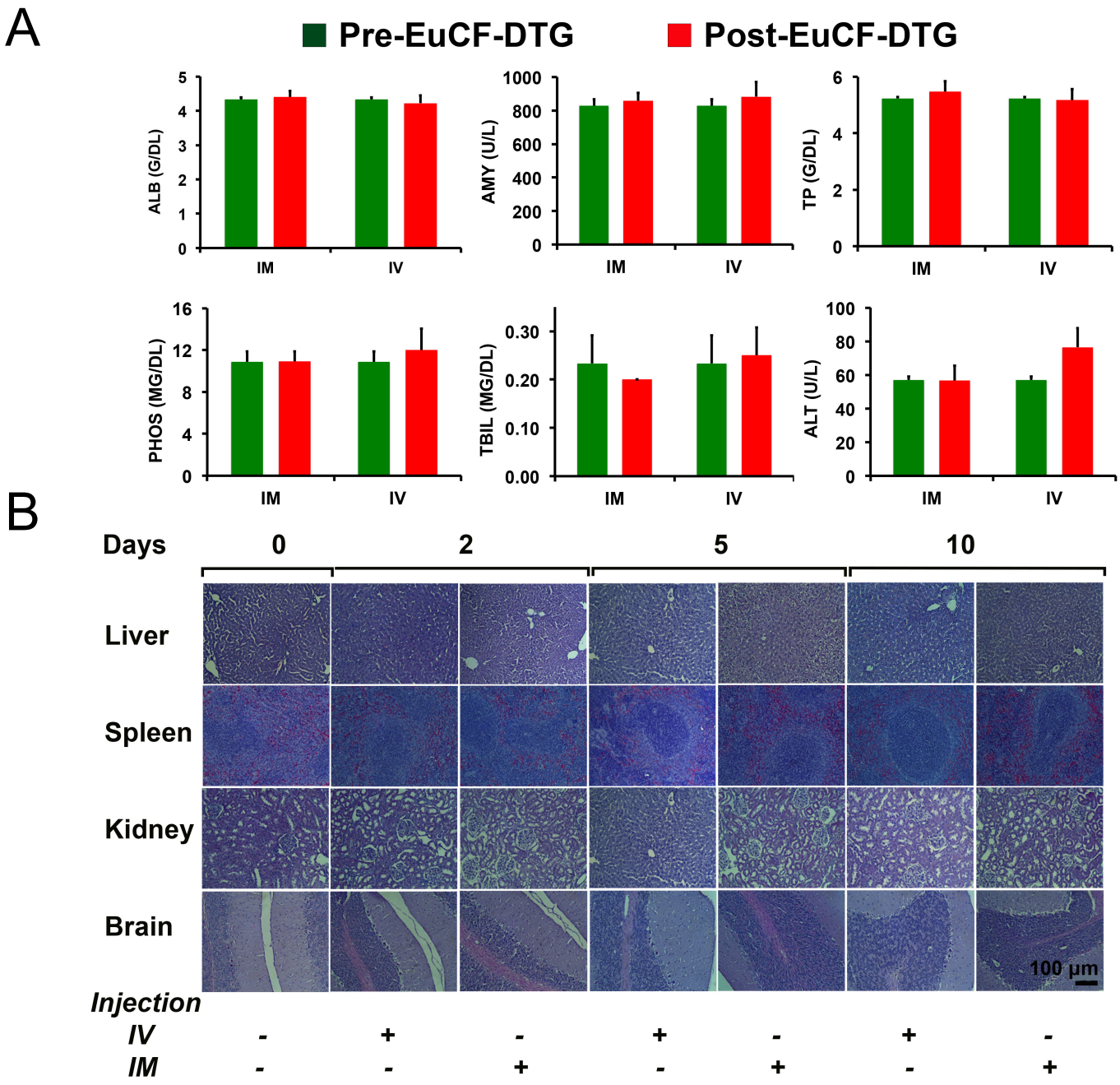

Figure S13: Evaluation of EuCF-DTG nanoparticle toxicity. (A) Hepatic, renal and pancreatic functions were analyzed in rats pre-and 5-days post-EuCF-DTG administration after IV or IM administration (ALB: Albumin, ALT: Alanine aminotransferase, TBIL: Total bilirubin, AMY: Amylase, PHOS: Phosphate, TP: Total protein) and (B) hematoxylin and eosin staining of rat tissues. Normal tissue histology was recorded in tissues in all animal groups. Images were captured with a 20 X magnification objective.

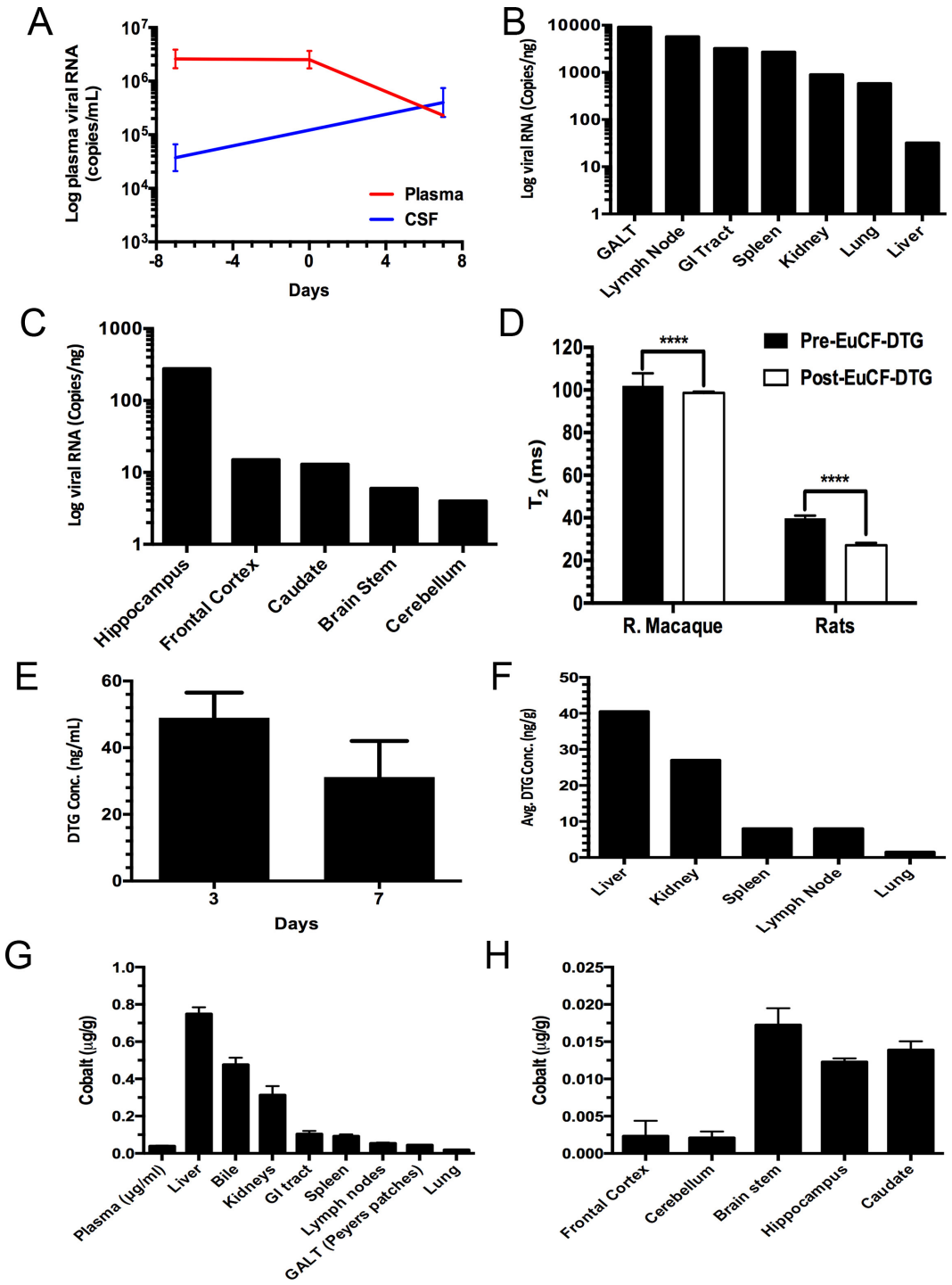

Figure S14: Biodistribution of EuCF-DTG nanoparticles in rhesus macaque tissues and effect on simian immunodeficiency virus (SIV) RNA loads. (A-C) plasma (results are shown as means ± SEM; n=3) and tissue viral RNA loads of SIV-infected rhesus macaque. (D) Rat and rhesus macaque T_2 relaxation in liver, (E-F) effect of EuCF-DTG treatment on plasma and comparison of DTG concentrations in post-mortem tissues measured by ICP-MS 5 days post IM injection of EuCF-DTG nanoparticles and (G-H) cobalt concentrations in the reticuloendothelial organs and brain regions at 2 mg iron/kg dosage.

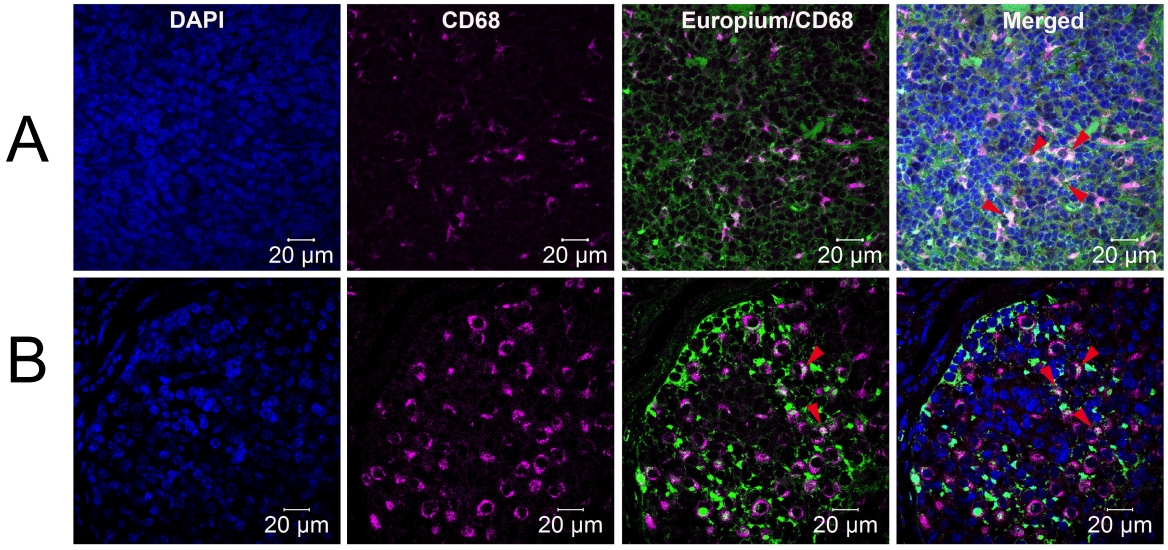

Figure S15: EuCF-DTG nanoparticle localization in rhesus macaque tissue macrophages by immunofluorescence staining. Representative tissues sections images by confocal microscopy; (A) spleen and (B) mesenteric lymph node 5 days after IM injection into rhesus macaque (2 mg/kg of iron). Where in DAPI (blue) stain indicates cell nuclei, EuCF-DTG nanoparticles (green, EuCF) and CD68 (magentas, macrophages). Co-localization of nanoparticles were seen in macrophages and indicated by red arrows in merged panel (light green). Images were captured with a 40X magnification objective. We observed co-localization of spleen macrophages with EuCF-DTG nanoparticles (green) in the tissues.

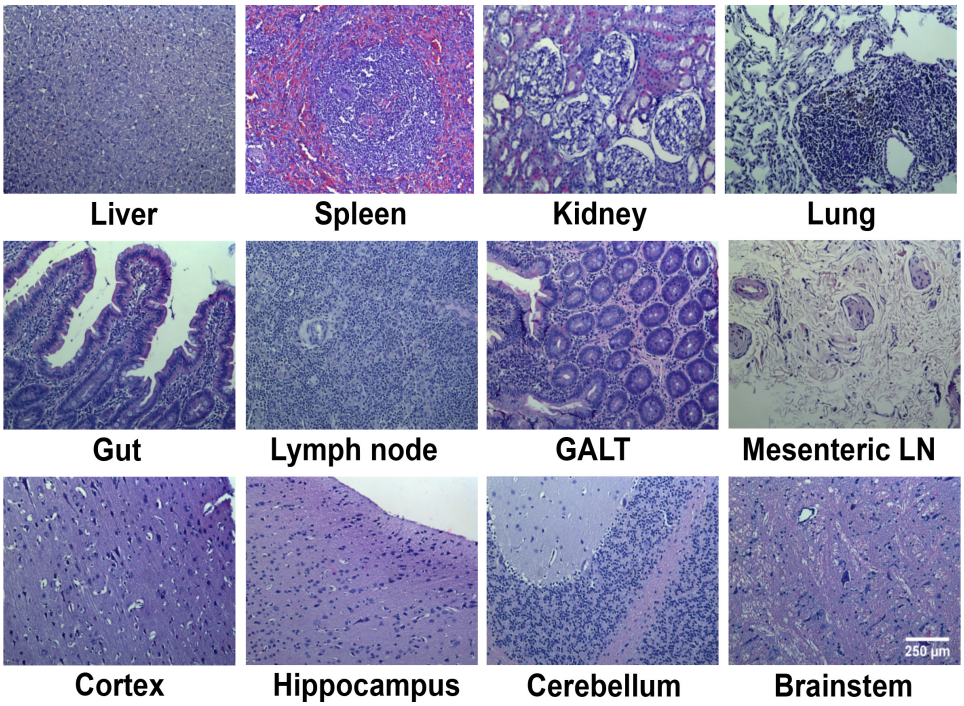

Figure S16: Histological evaluation of rhesus macaque tissues 5 days after EuCF-DTG injection. Tissue analysis was conducted in accordance with the guidelines of the Society of Toxicologic Pathology. No anomalies were observed. Tissues were collected from brain, liver, spleen, kidney, lung, lymph nodes (LN), gut-associated lymphoid tissue and several regions of brain. Haematoxylin and eosin stained images were illustrated at 20X magnification objective.

Table S1: Drug release kinetic parameters: Linear Correlation Coefficient (r^2) and rate constant (K) of the diffusion kinetic models applied to DTG release from EuCF-DTG nanoparticles (release data was consideration from first 6 days).

Kinetic models	Parameters	EuCF-DTG
Higuchi-equation	r^2	0.94094
	K_H	0.10122
Korsmeyer-Peppas	r^2	0.94094
	n	0.10122
	K_{HP}	0.63911
Elovich-equation	r^2	0.90371
	KE	0.28327
Parabolic-diffusion	r^2	**0.98918**
	Kp	0.12934
Bhaskar-Equation	r^2	**0.98842**
	K	-0.02143
Modified-Freundlich	r^2	0.80184
	K	-0.19458

Table S2: **Hematologic and metabolic profiles**. Effects of EuCF-DTG nanoparticles on biochemical and hematological parameters in rhesus macaques are illustrated.

Bleed No	Pre (day -5)	Day 0	Day 3 Post EuCF-DTG	Day 7 Post EuCF-DTG
WBC Count (x10E6/uL)	4.8	5.9	7.3	5.2
RBC Count (x10E6/uL)	5.38	5.46	6.28	5.92
Hemoglobin (g/dL)	10.2	12	11.8	11.3
Hematocrit (%)	32.9	38.2	38.6	36.8
MCV (fL)	61.2	70	61.5	62.2
MCHC (%)	31	31.4	30.6	30.7
RBC Distrib Width (%)	14.6	15.9	14.9	14.6
Platelet Count (x10E3/uL)	280	278	379	440
Type of Diff Done	Manual	Manual	Manual	Manual
Neutrophil Seg (%)	38	24	50	37
Neutrophil Band (%)	1	0	4	8
Lymphocyte (%)	54	54	38	38
Monocyte (%)	5	13	3	10
Eosinophil (%)	2	8	5	7
Basophil (%)	0	0	0	0
Nucleated RBC (/diff)	0	0	0	0
Absolute Neutrophil (x10E3/uL)	1.9	1.4	3.9	2.3
Absolute Lymphocyte (x10E3/uL)	2.6	3.2	2.8	2
Absolute Monocyte (x10E3/uL)	0.2	0.8	0.2	0.5
Absolute EOS (x10E3/uL)	0.1	0.5	0.4	0.4
Absolute BASO (x10E3/uL)	0	0.1	0	0
Normocytic	WNL	WNL	WNL	WNL
AST (U/L)	42		26	36
Alkaline Phosphatase (U/L)	162		190	180
Bilirubin Total (mg/dL)	0.2		0.2	0.1
Calcium (mg/dL)	8.2		8.3	8.7
Protein Total (g/dL)	6.8		6.9	7.1
Albumin (g/dL)	2.3		2.2	2.3
Glucose/Random (mg/dL)	31		57	62
Urea Nitrogen (mg/dL)	15		22	25
Creatinine (mg/dL)	0.67		0.61	0.66
Bun/ Creatinine Ratio (mgUN/mgCR)	22.4		36.1	37.9
Sodium (mmol/L)	144		140	142
Potassium (mmol/L)	4.6		3.6	3.9
Chloride (mmol/L)	111		104	107
Osmolality / Calc (mOsm/kg)	294		290	295
Carbon Dioxide (mmol/L)	23		24	22
Anion Gap (mmol/L)	10		12	13
ALT (U/L)	14		38	38